Composites Science and Technology 229 (2022) 109671

Contents lists available at ScienceDirect

Composites Science and Technology

journal homepage: www.elsevier.com/locate/compscitech

Bionic design and performance research of tracheal stent based on shape memory polycaprolactone

Wei Zhao [a], Zhipeng Huang [c], Liwu Liu [a], Wenbo Wang [c], Jinsong Leng [b], Yanju Liu [a,*]

[a] Department of Astronautical Science and Mechanics, Harbin Institute of Technology (HIT), P.O. Box 301, No. 92 West Dazhi Street, Harbin, 150001, China
[b] Center for Composite Materials and Structures, Harbin Institute of Technology (HIT), P.O. Box 3011, No. 2 YiKuang Street, Harbin, 150080, China
[c] The First Affiliated Hospital of Harbin Medical University, No. 23 You Zheng Street, Harbin, 150001, China

ARTICLE INFO

Keywords:
Shape memory polymer
Bionics design
Tracheal stent
Magnetic actuation

ABSTRACT

Trachea injury caused by tracheomalacia, stenosis or atresia can result in severe dyspnea, even asphyxia. With the development of trachea reconstruction technology, trachea stents have become an alternative treatment method. Here, we fabricated a kind of shape memory PCL/Fe_3O_4 composites (SMPC-PCL) by mixing different weight fractions of benzoyl peroxide and Fe_3O_4 nanoparticles. The addition of magnetic nanoparticles endowed SMPC-PCL with the capability of remote non-contact actuation, which exhibited unique advantages in minimally invasive implantation and adaptive ability. Further, based on fully observing the unique reticular structure of glass sponges, two types of biomimetics stents were designed and fabricated, and the mechanical properties were thoroughly investigated by experiments and finite element analysis. The minimally invasive implant performance and biological characterization were carried out to evaluate its availability. The excellent mechanical properties, minimally invasive implant performance and biological properties suggest the application potential in tracheal stents.

1. Introduction

Trachea function is vulnerable to tumors, trauma, and congenital diseases, resulting in trachea stenosis or tracheomalacia [1–3]. Tracheal injuries, stenosis, tumors and other diseases destroy the integrity and patency of the airway, leading to the loss of normal respiratory function, and directly endangering the lives of patients. For the treatment of tracheal diseases, there is still no safe and reliable method clinically, and the study of alternative tracheal stents has become an alternative method. Tracheal/bronchial prostheses, also known as tracheal stents, are commonly used to stabilize a collapsed trachea or assist in the healing or reconstruction of an injured trachea [4,5]. Depending on the fabrication materials, the tracheal stents can be classified as silicone stents, expandable metal stents [6] and degradable stents. Silicone stents are well tolerated and have sufficient stiffness to resist external compression. However, there is a risk of migration of silicone stents, which may make them more difficult to fix and require frequent replacement or repair [7]. Metal stents can be divided into self-expanding metal stents and fixed diameter stents. According to its processing technology, they are divided into covered and non-covered types. However, this kind of stent is unremovable and prone to hyperplasia, which may affect the second operation [8,9]. Biodegradable tracheal stents are generally fabricated by polylactic acid, polycaprolactone (PCL) or their copolymers. However, these stents need to be implanted into the body by surgical operation, and the implantation process is cumbersome, which greatly limits their applications.

For tracheal stents, the ideal design should have stable mechanical properties, equipping them with both strength and flexibility. They can not only provide support for softened or damaged tracheal tissues but also adapt to the deformation process of the trachea caused by breathing and swallowing. Moreover, for children, the stent needs to have the self-adaptive ability to gradually adjust its state with the growth of the trachea [10]. Therefore, not only the suitable materials but also the excellent design are the key to the trachea stents. In summary, how to implant these stents into the site of the lesion safely and keep them in the best working state for a long time is a common problem faced by trachea stents. Smart tracheal stents, characterized by stable mechanical properties, easy implantation, customization and adaptive ability, have gradually become the standard for the next generation of tracheal stents [4].

Shape memory polymer (SMP) can be designed into a desired permanent shape and programmed to obtain a temporary shape [11–13]. It

* Corresponding author.
E-mail address: yj_liu@hit.edu.cn (Y. Liu).

https://doi.org/10.1016/j.compscitech.2022.109671
Received 12 February 2022; Received in revised form 18 July 2022; Accepted 30 July 2022
Available online 31 August 2022

will maintain the temporary shape until the appropriate stimuli are applied again [14–17]. Depending on different actuation methods, SMP can be divided into thermally actuated SMP [18], light actuated SMP [19,20], magnetically actuated SMP [21,22], electrically actuated SMP [23], etc. Moreover, SMP has characteristics of easy programming, low density, easy processing and large deformation, which greatly enrich its application in the biomedical field [24–29]. As a type of SMP, shape memory poly (ε-caprolactone) (SMP-PCL) has been widely used in biomedical applications because of its excellent properties of non-toxic, environmentally friendly and biocompatible [30–37]. For example, Zhou et al. developed a kind of shape memory PCL (SMP-PCL) based nanofibers, which exhibited great potential for applications in tissue engineering as a multifunctional scaffold [38]. Furthermore, utilizing SMP-PCL, Zhou et al. developed a dynamically tunable, bioinspired micropatterned surface with a great capacity for inducing the formation of new blood vessels [39]. SMP-PCL based stents can be implanted into the body in a compact state and deployed to their initial shape under remote non-contact actuation, which will greatly facilitate the implantation process and enable it to adjust its state at any time.

In this work, shape memory poly (ε-caprolactone) composite (SMPC-PCL) was fabricated by mixing with different weight fractions of cross-linking agent-dibenzoyl peroxide and Fe_3O_4 nanoparticles. The mechanical properties and thermal-mechanical properties were investigated by TGA, DSC, DMA, and uniaxial tensile test. Furthermore, by analyzing the microstructure of the porous glass sponge, we designed two types of stents and fabricated them by SMPC-PCL. A series of mechanical and biological performance tests were carried out to evaluate the efficacy of stents. All the tests indicated that SMPC-PCL based stents exhibited excellent adaptive ability and could be implanted through minimally invasive surgery.

2. Materials and methods

2.1. Materials

The poly (ε-caprolactone) has a weight-average molecular weight of 112,000 Da, which was provided by the Centre for Composite Materials, Harbin Institute of Technology. The Fe_3O_4 nanoparticles with a 30 nm average diameter were commercially available from the Chengdu Institute of Organic Chemistry, Chinese Academy of Sciences. Benzoyl peroxide (BPO) was purchased from Tianjin Guangfu Fine Chemical Research Institute.

2.2. Thermal mechanical properties and mechanical properties of materials

SMPC-PCL were prepared by mixing with SMP-PCL, 10 wt% BPO and 10 wt%, 15 wt% and 20 wt% Fe_3O_4 nanoparticles, respectively. Subsequently, thermal gravimetric analysis (TGA), dynamic mechanical analysis (DMA), differential scanning calorimetry (DSC), thermal-mechanical cycle and durability tests were carried out to investigate the properties of SMPC-PCL. Finally, SMPC-PCL with 15 wt% Fe_3O_4 nanoparticles exhibited excellent properties and was used for the fabrication of the stents. (Detailed comparison of material properties can be found in Supporting Information, S1). Furthermore, uniaxial tensile experiments ans relaxation test were conducted to obtain the necessary parameters of the material for finite element simulation.

2.3. Design and fabrication of the stents

By imitating the structure of the siliceous venus flower basket, two series of tracheal stents were designed using the software of Solidworks 2018. The stents were fabricated by SMPC-PCL with 15 wt% Fe_3O_4 nanoparticles. Utilizing the laser cutter, the porous pattern was carved on a flat plate. Subsequently, the stents were obtained by crimping the structure and welding the two ends together.

2.4. Mechanical properties of the stent

The two types of stents were designed with an outer diameter of 18 mm, an inner diameter of 16 mm, and a length of 45 mm. By compression and three-point bending test, we investigated the radial compressive strength and flexural resistance of the stents. The tests were conducted at 37 °C, and the loading rates were 2 mm/min with a span length of 35 mm. Moreover, utilizing finite element software ABAQUS, we analyzed the change of the Poisson's ratio by uniaxial tensile simulation. Finally, the implantation and the deployment process of the stents were investigated by experiments and simulations. The deployment experiments of the stents were finished stimulated by the magnetic field with a frequency of 27.5 kHz and field strength of 4 kA m^{-1}.

3. Results

3.1. Thermal mechanical properties of SMPC-PCL with 15 wt% Fe_3O_4 nanoparticles

TGA curves of SMPC-PCL with 15 wt% Fe_3O_4 nanoparticle and 10 wt % BPO was shown in Fig. 1(a). The results showed that SMPC-PCL had good temperature resistance and no residue after decomposition. DMA results of SMPC-PCL were illustrated in Fig. 1(b). The x-coordinate value corresponding to the peak value of the loss angle was defined as the glass transition temperature (T_g). The glass transition process occurred in a range of temperatures, not limited to T_g. The T_g for SMPC-PCL was 54.64 °C, and the glass transition process started at 30 °C. Therefore, the tracheal stent prepared by SMPC-PCL can complete its minimally invasive implantation process and expand to its working state at a temperature close to the human body. The DSC results of SMPC-PCL was shown in Fig. 1(c), and the endothermic peak appeared at 52.28 °C.

3.2. Mechanical properties of SMPC-PCL with 15 wt% Fe_3O_4 nanoparticles

The thermal-mechanical cycle test curves of SMPC-PCL with 15 wt% Fe_3O_4 nanoparticles were illustrated in Fig. 2(a). 50% elongation was applied to the sample, and when the temperature was heated to 44 °C, the strain started to recover. The maximum load was 34.57 N when the temperature was cooled to −10 °C. SMPC-PCL exhibited excellent shape memory and shape recovery properties, which was the key to successful minimally invasive surgery.

The uniaxial tensile tests were conducted at temperatures of 20 °C, 30 °C, 40 °C and 50 °C by applying a strain of 0.016. Fig. 2(b) illustrated the elastic moduli of SMPC-PCL at different temperatures, which increased with the addition of Fe_3O_4 nanoparticles. The elastic moduli at 40 °C were 66 MPa, 77 MPa and 87 MPa of SMPC-PCL with 10 wt% Fe_3O_4, 15 wt% Fe_3O_4 and 20 wt% Fe_3O_4. SMPC-PCL had a higher elastic modulus at body temperature, while had a lower elastic modulus at 50 °C.

The durability tests of SMPC-PCL with 15 wt% Fe_3O_4 nanoparticles were shown in Fig. 2(c). By applying 5 mm deformation on the specimen, the maximum load was 45.6 N at temperatures of 40 °C and kept a constant. Due to the viscoelastic effect, the load-deformation curves were relatively discrete in the initial cycles. With the increase in cycle times, the dispersion phenomenon weakened gradually, and the load gradually tended to be stable. The residual deformation increased gradually with the increase of cyclic times, but it recovered to the initial shape by placing the sample in a high-temperature environment. After multiple loading-unloading cycles, the material had no damage and showed excellent fatigue resistance properties.

3.3. Bionics design and fabrication of the biomimetic stents

It should perfectly match the shape of the narrowed trachea and provide adequate support to keep the airway open after the stent is

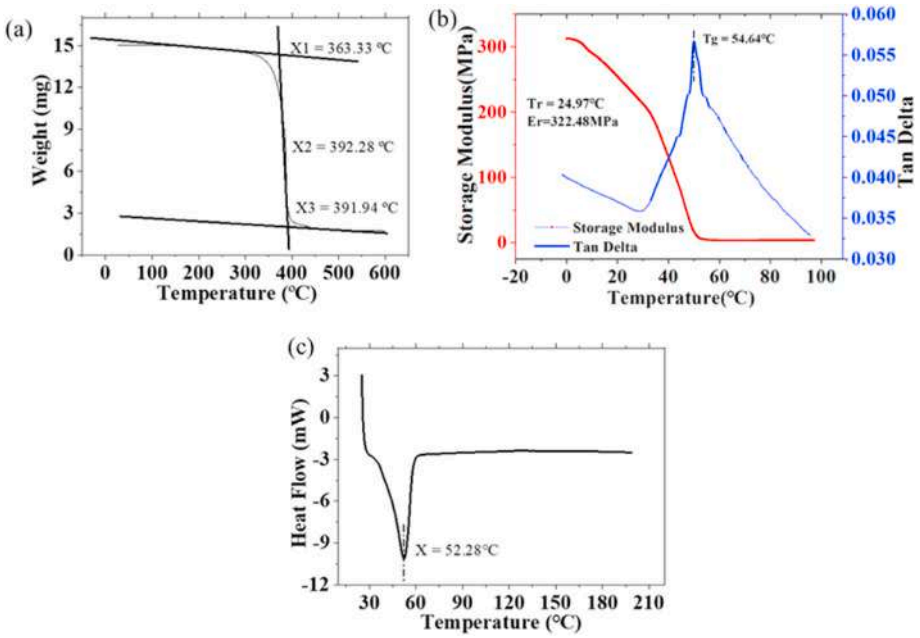

Fig. 1. Thermal mechanical properties of SMPC-PCL with 15 wt% Fe_3O_4 nanoparticles and 10% BPO (a) Thermal gravimetric analysis (b) Dynamic mechanical analysis (c) Differential scanning calorimetry.

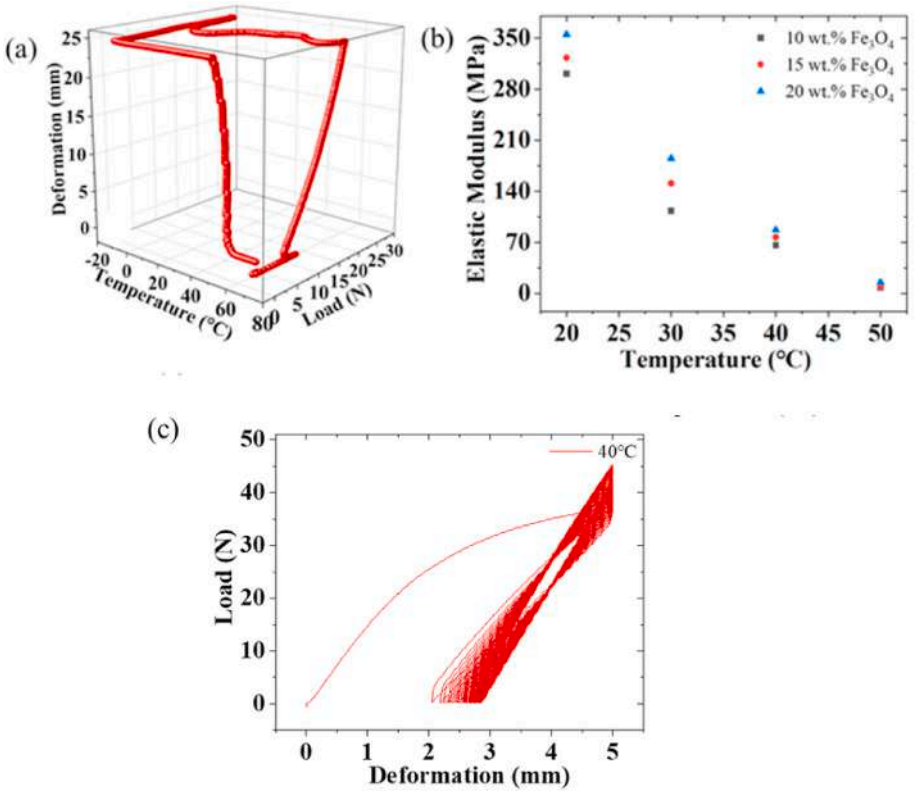

Fig. 2. Mechanical properties (a) Thermal-mechanical cycle tests of SMPC-PCL with 15 wt% Fe_3O_4 nanoparticles (b) Uniaxial tensile experiments (c) Durability tests of SMPC-PCL with 15 wt% Fe_3O_4 nanoparticles.

implanted into the lesion site. Moreover, the stents should be flexible enough to accommodate the complex deformation of the trachea caused by movements such as swallowing and breathing. Consequently, the structural design of the stent is also important for the function of the stent. Siliceous venus flower basket, also known as euplectella aspergillium, is an ancient creature that lives on the bottom of the sea. The geometric configuration of euplectella aspergillium is fairly unique, which is like a goblet or vase, and its skeleton is composed of radiating bone needles. The bone needles are crystal clear and interlaced, which are regularly arranged along the longitudinal, radial and spiral fibers. This porous structure, with its high toughness, strength and stability, can be firmly attached to the bottom of the ocean from being washed away

by ocean currents, and provide a strong barrier to protect the hidden fish and shrimp from being eaten. The essential features of lightweight, high strength and excellent flexibilities exhibited by the siliceous venus flower basket are exactly what stents need to have.

Consequently, by imitating the structure of the siliceous venus flower basket, we designed two series of tracheal stents as shown in Fig. 3(a) and (b). Design type I was obtained by imitating the porous structure of the glass sponge, which was simplified and improved based on the original octagonal hole in the siliceous venus flower. As shown in Fig. 3 (c), taking the outline of the octagonal hole as a reference, the surrounding triangular hole, hexagon hole, octagonal hole and their combination replaced the original octagonal hole. For stents I-1 and I-2, the octagonal hole was divided into five units, and the subunits of two adjacent units had different configurations. The two units were distributed alternately, and it not only ensured the strength of the stent but also achieved the purpose of being lightweight. Design type II was obtained by imitating the radiating bone needle structures and constructed by ligaments. The planar graph of the stents of series II was shown in Fig. 3(d). The four stents were constructed by different configurations of ligaments as shown in Fig. 3(e) and (f).

The fabrication process of biomedical stents was shown in Fig. 4 (a)-(d). Utilizing SMPC-PCL (15 wt% Fe_3O_4 nanoparticles) plate, the stent is obtained by rolling the flat plate into a tube and gluing the two ends of the plate together. The patterns with holes and ligaments were obtained by cutting an SMPC-PCL plate. Subsequently, the stents were obtained by crimping the structure and welding the two ends together. The fabricated stents are shown in Fig. 4(e).

3.4. Mechanical properties of the bionic stents

The uniaxial tensile properties of stents with different unit cells were simulated by ABAQUS. The viscoelastic module was adopted to describe the mechanical properties of PCL. The model parameter including Prony parameters and the elastic moduli was shown in Table S5, which was obtained by the uniaxial tensile test and relaxation test (See Supporting Information S1.4, Fig. S20). During the analysis process, one end of the stent was fixed and 50% deformation was applied to the other end. The transverse displacement cloud diagram of the tensile process was shown in Fig. 5. The change of the diameter at the middle cross-section during the tensile process was recorded. The longitudinal and radial strain can

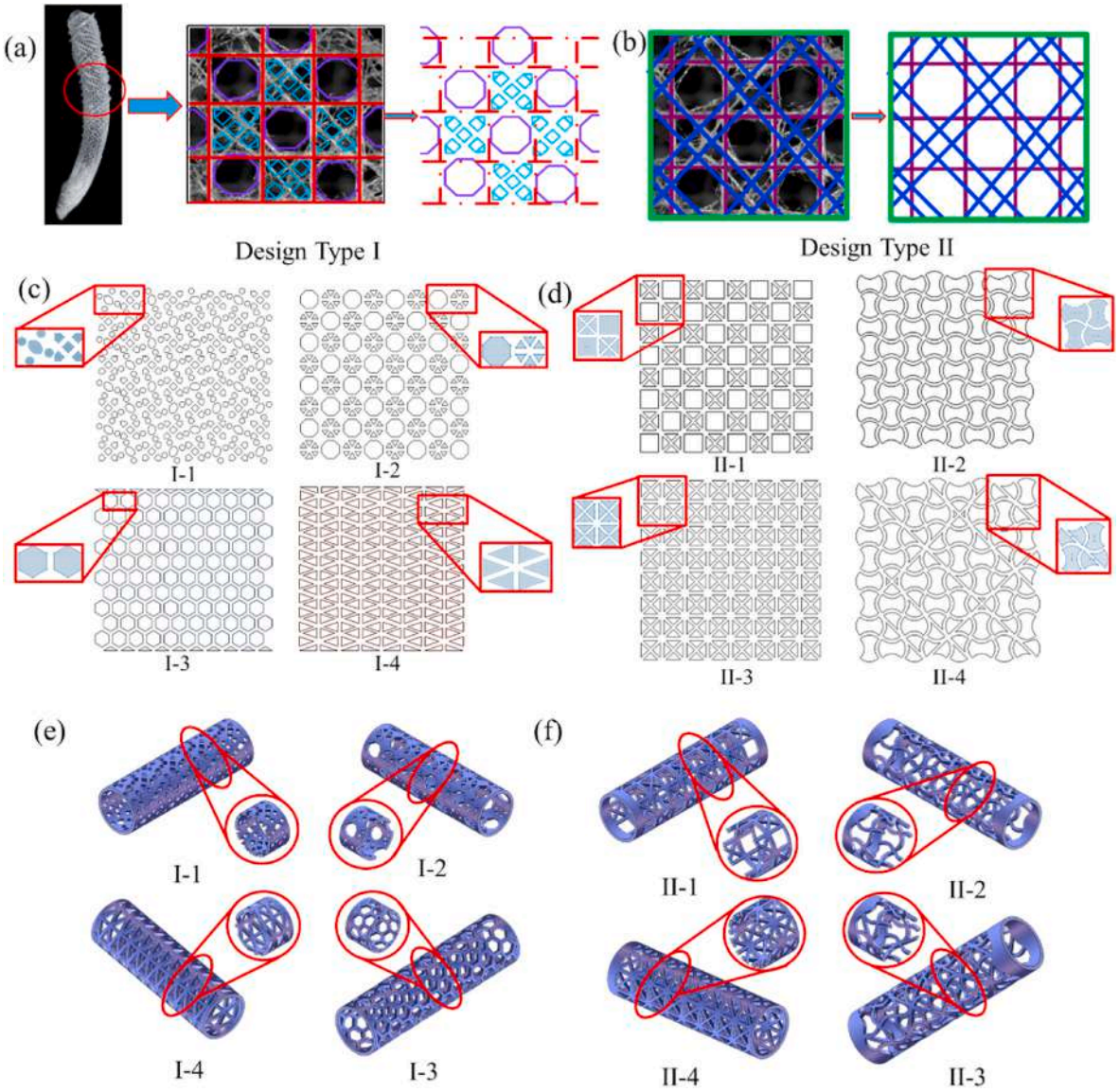

Fig. 3. Design of the bionic tracheal stents. Skeleton of the siliceous Venus flower basket, biomimetics design of (a) design type I and (b) design type II; (c) Planar configuration of design type I (d) Planar configuration of design type II (e) Three-dimensional configuration of the design type I (f) Three-dimensional configuration of the design type I.

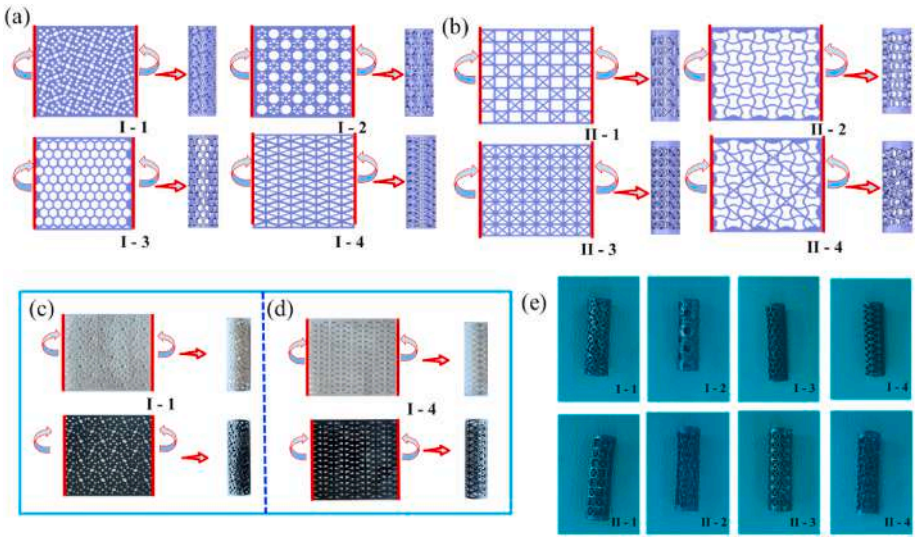

Fig. 4. Fabrication process of biomedical stents (a) Stents of design type I (b) Stents of design type II (c) Stent I - 1 (d) Stent I - 4 (e) Display of the stents.

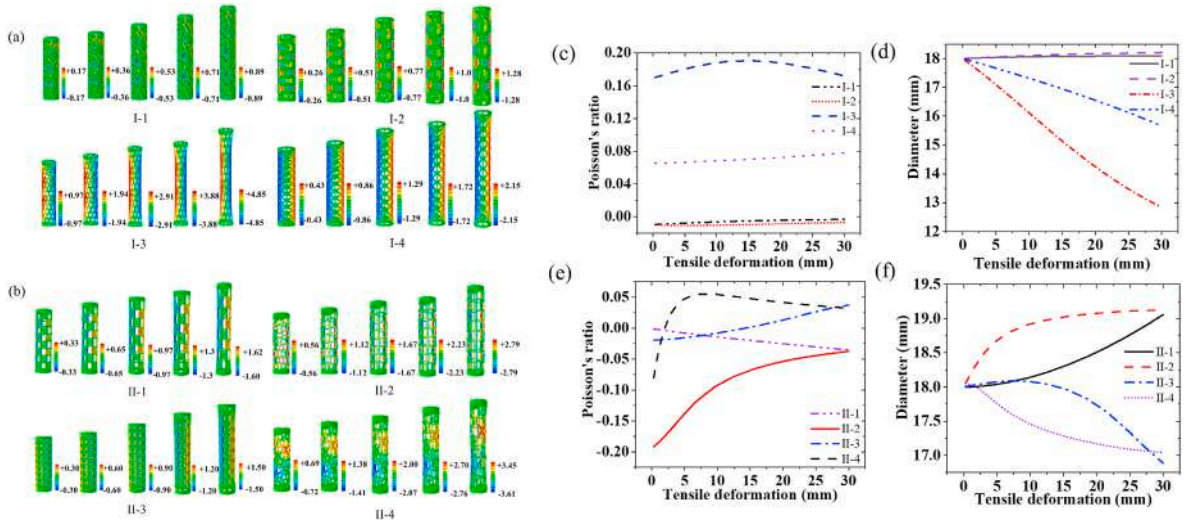

Fig. 5. Finite element analysis of the uniaxial tensile properties (a) Transverse aberration programs of design type I stents (b) Transverse aberration programs of design type II stents (c) Poisson's ratio of the design Type I stents changes with deformation (d) Diameter of the design Type I stents changes with deformation (e) Poisson's ratio of the design Type II stents changes with deformation (f) Diameter of the design Type II stents changes with deformation.

be expressed as:$\varepsilon_L = (L_{final} - L_{initial})/L_{initial} \times 100\%$, $\varepsilon_r = (D_{final} - D_{initial})/D_{initial} \times 100\%$. Further, the Poisson's ratio can be obtained: $\nu = -\varepsilon_r/\varepsilon_L$.

From Fig. 5 (a), (c) and (d), it can be seen that the Poisson's ratio of stents I-1, I-2 is negative, and the diameter of the stent increases with tensile deformation. The Poisson's ratio of I-3 and I-4 is positive, and with the increase of the deformation, the diameter decrease gradually. From Fig. 5(b), (e) and (f), it can be seen that Poisson's ratio of design type II under small deformation is negative. The Poisson's ratio of stents II-1 and II-2 is negative within 50% deformation. The Poisson's ratio of stents II-3 and II-4 gradually changes from negative to positive with the increase of deformation.

The compressive and three-point bending tests were conducted to characterize the compression resistance and flexibility of the structures. Firstly, we investigated the bending property of the planar configuration as shown in Fig. 6 (a) and (b). The results indicated that the bending strength of design type I was higher than design type II. The bending strengths of plates I-1 and I-2 were the highest, followed by I-3, I-4, II-1 and II-3, and II-2 and II-4 were the lowest.

The compressive properties of the stents of design type I and type II with a wall thickness of 1.5 mm were shown in Fig. 6(c) and (d), respectively. The results indicated that there was little difference in the radial support strength of the stents I-1, I-2 and I-4. However, due to the larger porosity of stent I-3, it exhibited weaker radial strength. At 20 N compression load, the deformations of the four stents were 2.1 mm of I-1, 2.2 mm of I-2, 6 mm of I-3, and 2.3 mm of I-4, respectively. For stents of design type II, the differentiation of radial strength is obvious. The radial strength of stents II-1 and II-3 was higher than stents II-2 and II-4. At 20 N compression load, the deformations of the four stents were 1.7 mm of II-1, 5.6 mm of II-2, 1.6 mm of II-3, and 5.6 mm of II-4, respectively. The radial support strengths of II-1 and II-3 were similar, while II-2 and II-4 were similar except for a slight difference at the later loading stage. Overall, stents II-2 and II-4 are suitable for softened trachea requiring low support strength, while other stents are suitable for softened trachea requiring high support strength.

The three-point bending test results were shown in Fig. 6 (e)–(h). From Fig. 6(e), it can be seen that stent I-1 had the highest bending strength, followed by stent I-2 and stent I-4. When the deformation was

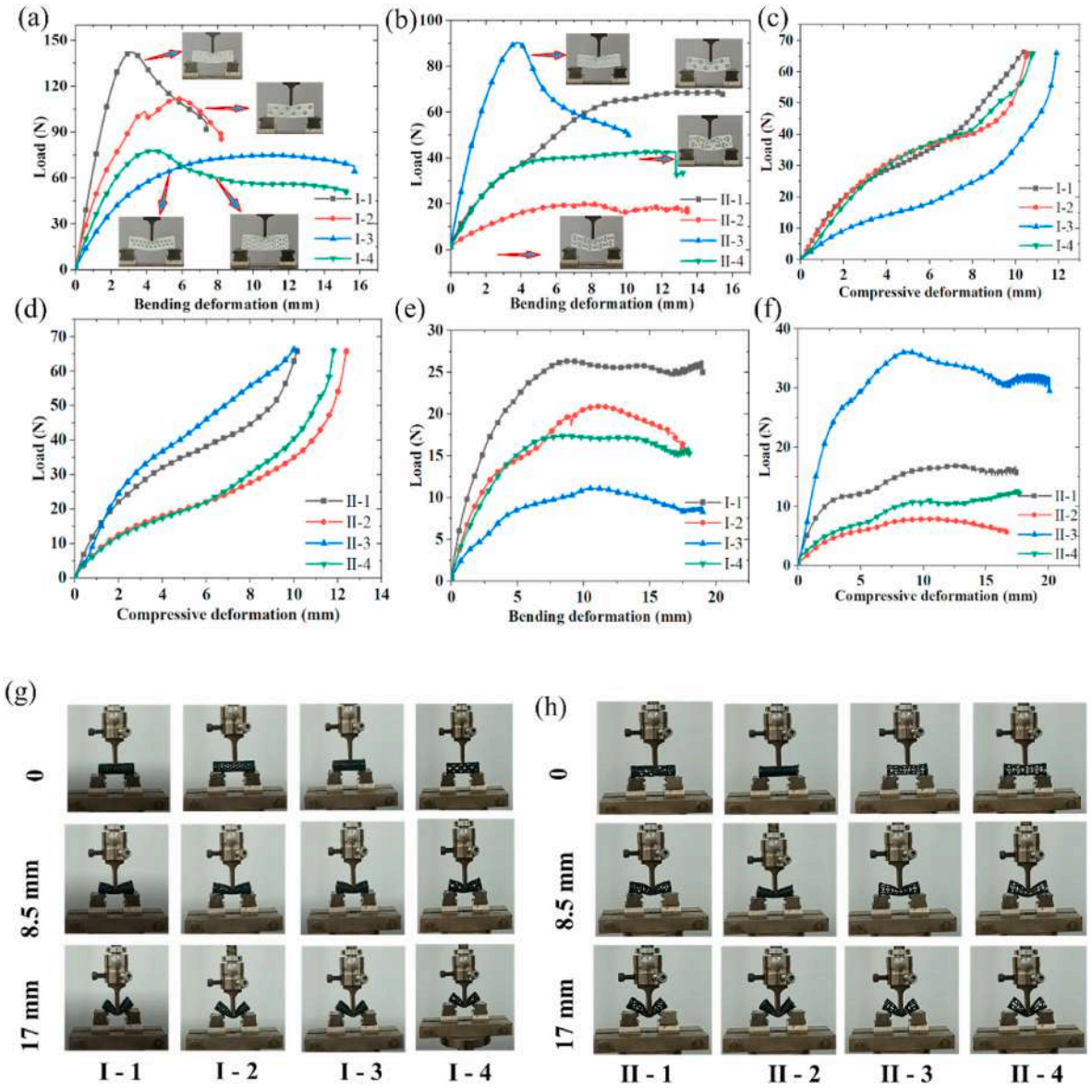

Fig. 6. Mechanical properties test of the stents (a) Three-point bending test of the planar configuration of the stents, design type I and (b) design type II; (c) Compressive test of design type I (d) Compressive test of design type II (e) Three-point bending test of design type I (f) Three-point bending test of design type II (g) Configuration evolution process of design type I during loading (h) Configuration evolution process of design type II during loading.

10 mm, the loads were about 26.1 N, 20.5 N, 10 N and 17.2 N for I-1, I-2, I-3 and I-4, respectively. The configurations of the stents under different deformations can be seen in Fig. 6(g). For type II stents, except for the bending strength of stent II-3 was relatively large, the rest were relatively small. When the deformation was 10 mm, the loads were about 16.3 N, 7.8 N, 35.2 N and 10.7 N for I-1, I-2, I-3 and I-4, respectively. Therefore, the results indicated that stent I-3, stent II-2 and stent II-4 had the best flexibility under the same load. The thickness of the stents is 1.5 mm, and the mechanical properties can be controlled by adjusting the thickness of the wall. However, how to select the appropriate strength needs to be analyzed according to the lesion location and the mechanical properties of surrounding tissues.

3.5. Simulation and experiments of the deployment process

The magnetic actuation is considered the most elegant actuated method to trigger the deployment of SMP-based biomedical devices, which has been verified by many applications in vivo and in vitro [40, 41]. The deployment process of the stents was simulated by the finite element method. Firstly, two endpoints of orthogonal diameters were selected on the cross-section of the stent. Based on this connection line, the stent was deformed by about 7.5 mm to obtain the tracheal stent configuration in the folded state as shown in Fig. 7(a) and (b). After folding, the stents shrank into an X shape, which greatly reduced the contact area with the implanted device in the process of implantation. When implanted into the lesion location, the stents gradually returned to their original shape stimulated by the magnetic field. Through simulation, it can be found that the shape recovery ratio of the stents is about 95%.

Furthermore, another folding type was used to verify the implantation and expansion process of the stents as shown in Fig. 8. To facilitate the implantation, the stents were folded and rolled up, and then gradually returned to their original shape actuated by the magnetic field. The actuation efficiency of the alternative magnetic field with different field intensity and frequency was investigated to determine the optimal working conditions (See Supporting Information S1.5). It can be concluded that the recovery time decreased gradually with the increase in the weight fraction of Fe_3O_4 nanoparticles while the actuation

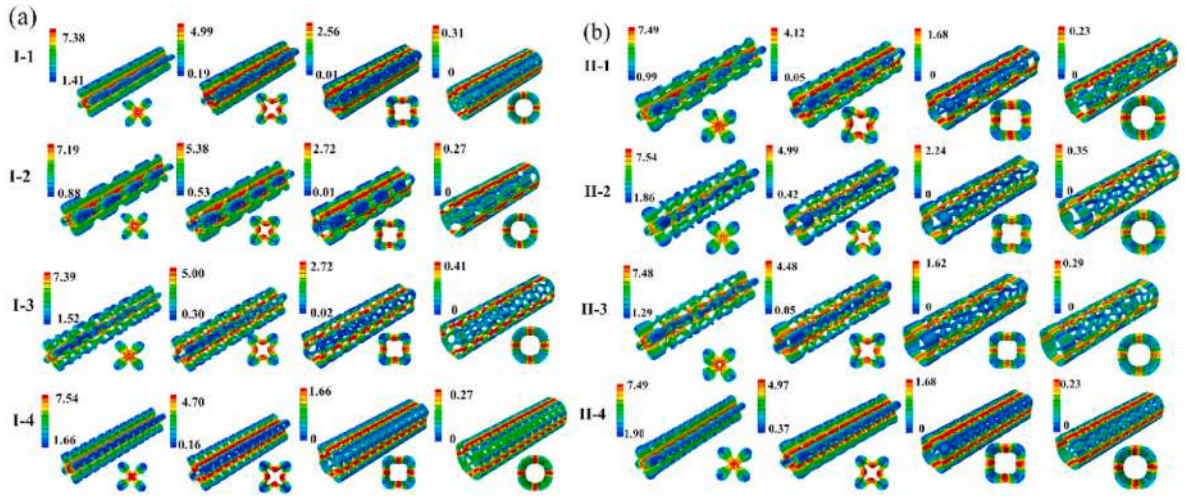

Fig. 7. Simulation of the deployment process (a) Stents of design type I (b) Stents of design type II.

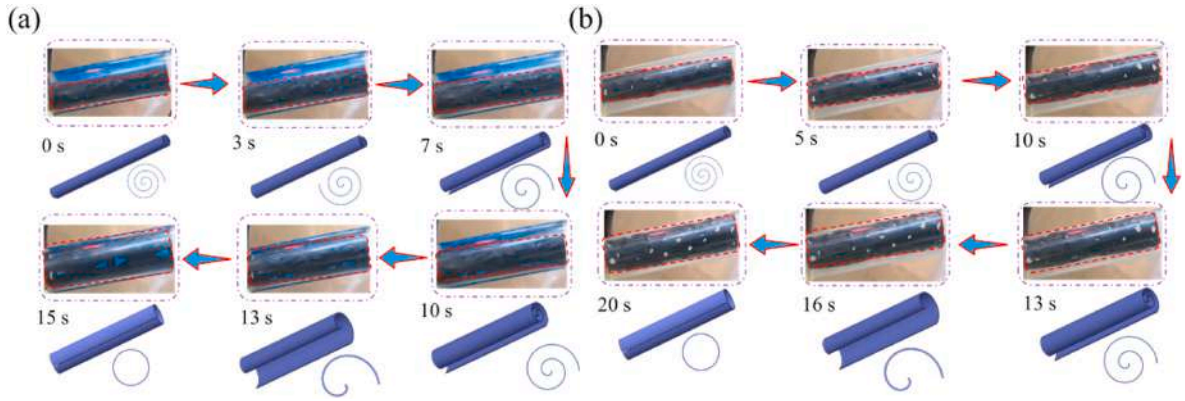

Fig. 8. Shape recovery process of (a) stents S–I and (b) S-II stimulated by the magnetic field (The red rectangles were the outline of the stent). (For interpretation of the references to colour in this figure legend, the reader is referred to the Web version of this article.)

efficiency gradually decreased with the increase of magnetic field frequency. Finally, the stents fabricated with SMPC-PCL (15 wt% Fe_3O_4 nanoparticles) were placed under an alternating magnetic field with a frequency of 27.5 kHz and an intensity of 4 kA m^{-1}. The results indicated that stents I-1 and II-4 completely recovered to their initial shape and fitted to the outer wall of the trachea model in 15 s and 20 s, which fully demonstrated the minimally invasive implantation property of the stents.

4. Discussion

To date, conventional tissue engineering stents have been limited to static structures and do not have the self-adaptive ability. For children, the stents will eventually develop into a restrictive structure due to their lack of self-adaptive ability. To avoid the second operation and reduce the patient's pain, the next generation of stents should be endowed with the self-adaptive ability to adapt to tissue growth or change, or the stent gradually degrades after endothelialization.

The purpose of this study is to design and fabricate a new kind of porous tracheal stents, which can be implanted into the body through minimally invasive surgery. Moreover, shape memory performance allows the stents to adjust their fixed state in time and to provide suitable support for the trachea. They exhibit certain flexibility to adapt to the deformation of the trachea. The adaptive performance of stents is manifested in two aspects. First, the stents can adjust their state and keep the optimal support state by applying suitable stimulus utilizing SME. Furthermore, based on the negative Poisson's ratio performance, the stents expand under the tensile load, which will avoid blocking when subjected to a deformation caused by the trachea.

To select and design a suitable porous structure, we observed and analyzed the structure of the glass sponge, and found that it had the characteristics of high strength and strong stability. Therefore, two types of stents were obtained by bionics design of the porous structures and the bone needles. Through mechanical analysis, it is found that stents of design type I had positive Poisson's ratios, while design Type II had negative Poisson's ratios.

During normal breathing or neck movement, the length of the trachea can increase by 20% in healthy adults and 46% in newborns. Furthermore, children's trachea will exert tensile load on the stent during the growth process, and the supporting area of the stent will increase accordingly under the action of tensile load. For the stents of design type I, Poisson's ratios of stent I-1 and stent I-2 were close to zero and almost unchanged during deformation. The diameter of the stent with a negative Poisson's ratio will increase when it is stretched. The Poisson's ratio of the stents ranges from −0.20 to 0.16. However, the selection of such stents should be based on the full study of the mechanical properties of the trachea at different parts.

Traditional stents are implanted into the body by surgical operation, which is complicated and causes great pain to patients. To facilitate the implantation process and adjustment of the support state, the stents fabricated in this paper have magnetic response performance, which can be compacted before implantation and implanted into the body in

minimally invasive surgery. After that, the stent expands to its initial shape to provide support for the trachea stimulated by the magnetic field. Besides, the supporting state of the stent can be readjusted by applying a magnetic field again. Fig. 8 verified the unfolding process of the stent actuated by the magnetic field.

Although we verified the mechanical properties, flexibility and biocompatibility of the shape memory tracheal stents in vitro, these tests could not truly reflect the function and support effect in vivo. Due to the complex mechanical and biochemical environment in the organism, stents will face greater challenges. In the next work, several questions need to be validated in animal models. For example, whether the stent can be deployed smoothly in the body actuated by magnetic fields. If it can maintain the optimal support state in the body through timely regulation in vivo, and whether it can regulate its state as the child's trachea grows. The stent show great potential in adaptive ability and minimally invasive implantation, which needs to be further studied.

5. Conclusions

To prepare and fabricate shape memory tracheal stents with self-adaptive ability, we designed them from two perspectives: material and structure. Firstly, we fabricate a kind of PCL-based SMPC by mixing different weight fractions of BPO and Fe_3O_4 nanoparticles. Through a series of mechanical properties tests, we confirmed the shape memory effect and durability performance of the material. Subsequently, based on fully observing the unique reticular structure of glass sponges, two design types of stents were designed and fabricated by compression molding and laser cutting. The mechanical properties and minimally invasive implant properties of the stents were characterized by experiments and simulations. The compressive tests and three-point bending tests indicated the excellent radial strength and flexural strength of the stents. Moreover, the stents were successfully deployed actuated by the magnetic field. The suitable strength, flexibility, SME and excellent biological properties represent additional possibilities to explore in the biomedical stent.

CRediT authorship contribution statement

Wei Zhao: Conceptualization, Methodology, Investigation, Visualization, Writing – original draft, Writing – review & editing, Validation. **Zhipeng Huang:** Methodology, Investigation, Visualization, Writing – review & editing, Validation. **Liwu Liu:** Investigation, Visualization, Writing – review & editing, Validation. **Wenbo Wang:** Investigation, Writing – review & editing, Validation. **Jinsong Leng:** Funding acquisition, Supervision, Methodology, Investigation, Writing – review & editing, Validation. **Yanju Liu:** Funding acquisition, Supervision, Methodology, Investigation, Writing – review & editing, Validation.

Declaration of competing interest

The authors declare that they have no known competing financial interests or personal relationships that could have appeared to influence the work reported in this paper.

Data availability

No data was used for the research described in the article.

Acknowledgment

This work was supported by the National Natural Science Foundation of China (Grant No. 12072094 and 12172106), Heilongjiang Touyan Innovation Team Program and the Fundamental Research Funds for the Central Universities (No. IR2021106 and IR2021232).

Appendix A. Supplementary data

Supplementary data to this article can be found online at https://doi.org/10.1016/j.compscitech.2022.109671.

References

[1] J.P. Liu, X.H. Yao, Z.W. Wang, J. Ye, C.C. Luan, Y. He, H. Lin, J.Z. Fu, A flexible porous chiral auxetic tracheal stent with ciliated epithelium, Acta Biomater. 124 (2021) 153–165.
[2] X.F. Xiong, L. Xu, L. Fan, D.Y. Cheng, B.X. Zheng, Long-term follow-up of self-expandable metallic stents in benign tracheobronchial stenosis: a retro-spective study, BMC Pulm. Med. 19 (1) (2019) 1–10.
[3] J. Xu, H.X. Ong, D. Traini, M. Byrom, J. Williamson, P.M. Young, The utility of 3D-printed airway stents to improve treatment strategies for central airway obstructions, Drug Dev. Ind. Pharm. 45 (1) (2019) 1–10.
[4] M. Zarek, N. Mansour, S. Shapira, D. Cohn, 4D printing of shape memory-based personalized endoluminal medical devices, Macromol. Rapid Commun. 38 (2) (2017), 1600628.
[5] J. H Park, J.K. Yoon, J.B. Lee, Y.M. Shin, K.W. Lee, S.W. Bae, J.H. Lee, J.J. Yu, C. R. Jung, Y.N. Youn, H.Y. Kim, D.H. Kim, Experimental tracheal replacement using 3-dimensional bioprinted artificial trachea with autologous epithelial cells and chondrocytes, Sci. Rep. 9 (1) (2019) 1–11.
[6] S.K. Avasarala, L. Freitag, A.C. Mehta, Metallic endobronchial stents: a contemporary resurrection, Chest 155 (6) (2019) 1246–1259.
[7] D. Makris, C.H. Marquette, Tracheobronchial stenting and central airway replacement, Curr. Opin. Pulm. Med. 13 (4) (2007) 278–283.
[8] T. Wang, J. Zhang, J. Wang, Y.H. Pei, X.J. Qiu, Y.L. Wang, Paclitaxel drug-eluting tracheal stent could reduce granulation tissue formation in a canine model, Chin. Med. J. 129 (22) (2016) 2708–2713.
[9] Y.H. Li, M.D. Li, X.F. Wang, Y.H. Wang, C. Li, Y.N. Zhao, Z.N. Li, J.J. Chen, J. Li, K. W. Ren, Z.M. Li, J.Z. Ren, X.W. Han, Q. Li, Comparison of three kinds of self-expandable metallic stents induced granulation tissue hyperplasia in the rabbit trachea, Sci. Rep. 11 (2021), 23115.
[10] R.J. Morrison, S.J. Hollister, M.F. Niedner, M.G. Mahani, A.H. Park, D.K. Mehta, R. G. Ohye, G.E. Green, Mitigation of tracheobronchomalacia with 3D-printed personalized medical devices in pediatric patients, Sci. Transl. Med. 7 (285) (2015), 285ra64-285ra64.
[11] W. Zhao, L.W. Liu, J.S. Leng, Y.J. Liu, Thermo-mechanical behavior prediction of shape memory polymers based on multiplicative decompositions of the deformation gradient, Mech. Mater. 143 (2020), 103263.
[12] Y.Q. Mao, F. Chen, S.J. Hou, H.J. Qi, K. Yu, A viscoelastic model for hydrothermal activated malleable covalent network polymer and its application in shape memory analysis, J. Mech. Phys. Solid. 127 (2019) 239–265.
[13] W. Zhao, N. Li, L.W. Liu, J.S. Leng, Y.J. Liu, Origami derived self-assembly stents fabricated via 4D printing, Compos. Struct. 293 (2022), 115669.
[14] L. Chen, Y. Zhang, H.T. Ye, G.H. Duan, H.G. Duan, Q. Ge, Z.L. Wang, Color-changeable four-dimensional printing enabled with ultraviolet-curable and thermochromic shape memory polymers, ACS Appl. Mater. Interfaces 13 (15) (2021) 18120–18127.
[15] W. Zhao, L.W. Liu, J.S. Leng, Y.J. Liu, Thermo-mechanical behavior prediction of particulate reinforced shape memory polymer composite, Compos. Part B-Eng. 179 (2019), 107455.
[16] D.W. Hanzon, H.B. Lu, C.M. Yakacki, K. Yu, Influence of mechanically-induced dilatation on the shape memory behavior of amorphous polymers at large deformation, Mech. Time-Dependent Mater. 23 (1) (2018) 1–21.
[17] W. Zhao, J. Zhu, L.W. Liu, J.S. Leng, Y.J. Liu, Analysis of small-scale topology and macroscale mechanical properties of shape memory chiral-lattice metamaterials, Compos. Struct. 262 (2021), 113569.
[18] Y.L. Fang, X.S. Du, Y.X. Jiang, Z.L. Du, P.T. Pan, X. Cheng, H.B. Wang, Thermal-driven self-healing and recyclable waterborne polyurethane films based on reversible covalent interaction, ACS Sustain. Chem. Eng. 6 (11) (2018) 14490–14500.
[19] H.N. Wang, L. Fang, Z. Zhang, J. Epaarachchi, L.Y. Li, X. Hu, C.H. Lu, Z.Z. Xu, Light-induced rare earth organic complex/shape-memory polymer composites with high strength and luminescence based on hydrogen bonding, Compos. Part A-Appl. 125 (2019), 105525.
[20] T.J. Wang, J. Zhao, C.X. Weng, T. Wang, Y.Y. Liu, Z.P. Han, Z. Zhang, A bidirectionally reversible light-responsive actuator based on shape memory polyurethane bilayer, Compos. Part A-Appl. 144 (2021), 106322.
[21] C. Meiorin, D.G. Actis, F.E. Montoro, O.M. Londoño, M.I. Aranguren, D. Muraca, P. M. Zélis, M. Knobel, M.A. Mosiewicki, Magnetic remote activation of shape recovery in nanocomposites based on tung oil and styrene, Phys. Status Solidi 215 (24) (2018), 1800311.
[22] W. Zhao, L.W. Liu, Y.J. Liu, J.S. Leng, Porous bone tissue scaffold concept based on shape memory PLA/Fe_3O_4, Compos. Sci. Technol. 203 (2021), 108563.
[23] X.Y. Huang, P.M. Sarmad, K. Dong, R.Q. Li, T.J. Chen, X.L. Xiao, Tracing evolutions in electro-activated shape memory polymer composites with 4D printing strategies: a systematic review, Compos. Part A-Appl. 147 (2021), 106444.
[24] W. Zhao, F.H. Zhang, J.S. Leng, Y.J. Liu, Personalized 4D printing of bioinspired tracheal scaffold concept based on magnetic stimulated shape memory composites, Compos. Sci. Technol. 184 (2019), 107866.

[25] S.M. Montgomery, X. Kuang, C.D. Ar mstrong, H.J. Qi, Recent advances in additive manufacturing of active mechanical metamaterials, Curr. Opin. Solid. St. M. 24 (5) (2020), 100869.
[26] J. Wang, Q.L. Zhao, Y.L. Wang, Q. Zeng, T.Z. Wu, X.M. Du, Self-unfolding flexible microelectrode arrays based on shape memory polymers, Adv. Mater. Technol. 4 (11) (2019), 1900566.
[27] Q.L. Zhao, J. Wang, Y.L. Wang, H.Q. Cui, X.M. Du, A stage-specific cell-manipulation platform for inducing endothelialization on demand, Natl. Sci. Rev. 7 (3) (2020) 629–643.
[28] Y.C. Zhang, J.L. Hu, R.Q. Xie, X. Zhao, A programmable, fast-fixing, osteo-regenerative, biomechanically robust bone screw, Acta Biomater. 103 (2020) 293–305.
[29] T.J. Esworthy, S.D. Miao, S.J. Lee, X. Zhou, H.T. Cui, Y.Y. Zuo, L.J.G. Zhang, Advanced 4D-bioprinting technologies for brain tissue modeling and study, Int. J. Smart Nano Mat. 10 (3) (2019) 177–204.
[30] I. Navarro-Baena, J.M. Kenny, L. Peponi, Thermally-activated shape memory behaviour of bionanocomposites reinforced with cellulose nanocrystals, Cellulose 21 (6) (2014) 4231–4246.
[31] T. Tsujimoto, T. Takayama, H. Uyama, Biodegradable shape memory polymeric material from epoxidized soybean oil and polycaprolactone, Polymers 7 (10) (2015) 2165–2174.
[32] F.H. Zhang, T.Y. Zhou, Y.J. Liu, J.S. Leng, Microwave synthesis and actuation of shape memory polycaprolactone foams with high speed, Sci. Rep. 5 (2015), 11152.
[33] W. Yan, L. Fang, U. Noechel, K. Kratz, A. Lendlein, Influence of deformation temperature on structural variation and shape memory effect of a thermoplastic semi-crystalline multiblock copolymer, Express Polym. Lett. 9 (7) (2015) 624–635.
[34] M. Kashif, B.M. Yun, K.S. Lee, Y.W. Chang, Biodegradable shape-memory poly (ε-caprolactone)/polyhedral oligomeric silsequioxane nanocomposites: sustained drug release and hydrolytic degradation, Mater. Lett. 166 (2016) 125–128.
[35] I. Navarro-Baena, J.M. Kenny, L. Peponi, Crystallization and thermal characterization of biodegradable tri-block copolymers and poly(ester-urethane)s based on PCL and PLLA, Polym. Degrad. Stabil. 108 (2014) 140–150.
[36] W. Zhao, L.W. Liu, F.H. Zhang, Y.J. Liu, J.S. Leng, Shape memory polymers and their composites in biomedical applications, Mat. Sci. Eng. C-Mater. 97 (2019) 864–883.
[37] T. Xiang, J.W. Hou, H. Xie, X. Liu, T. Gong, S.B. Zhou, Biomimetic micro/nano structures for biomedical applications, Nano Today 35 (2020), 100980.
[38] T. Gong, K. Zhao, X. Liu, L.X. Lu, D. Liu, S.B. Zhou, A dynamically tunable, bioinspired micropatterned surface regulates vascular endothelial and smooth muscle cells growth at vascularization, Small 12 (2016) 5769–5778.
[39] T. Gong, W.B. Li, H.M. Chen, L. Wang, S.J. Shao, S.B. Zhou, Remotely actuated shape memory effect of electrospun composite nanofibers, Acta Biomater. 8 (3) (2012) 1248–1259.
[40] H.Q. Wei, Q.W. Zhang, Y.T. Yao, L.W. Liu, Y.J. Liu, J.S. Leng, Direct-write fabrication of 4D active shape-changing structures based on a shape memory polymer and its nanocomposite, ACS Appl. Mater. Interfaces 9 (1) (2017) 876–883.
[41] L.Q. Ren, B.Q. Li, Z.Y. Song, Q.P. Liu, L. Ren, X.L. Zhou, Bioinspired fiber-regulated composite with tunable permanent shape and shape memory properties via 3d magnetic printing, Compos. B Eng. 164 (2019) 458–466.